ChemElectroChem

Chemistry Europe
European Chemical Societies Publishing
ChemElectroChem

RESEARCH ARTICLE OPEN ACCESS

Selective Electrochemical sp^3 C—O Bond Hydrogenolysis: From Model Compounds to Lignin

Miquel Molina-García[1] | Antonio Doménech-Carbó[2] | Marta Mon[1] | Antonio Leyva-Pérez[1]

[1]Instituto de Tecnología Química (Universitat Politècnica de València–Agencia Estatal Consejo Superior de Investigaciones Científicas), Valencia, Spain | [2]Departament de Química Analítica, Universitat de Valencia, Valencia, Spain

Correspondence: Marta Mon (marmoco@itq.upv.es) | Antonio Leyva-Pérez (anleyva@itq.upv.es)

Received: 5 February 2026 | **Accepted:** 9 February 2026

Keywords: C—O bond cleavage | electrosynthesis | hydrogenolysis | lignin depolymerization | selective O—H and C—H bond formation

ABSTRACT

The valorization of lignin into aromatic products is currently one of the most relevant challenges in sustainable chemistry. Here, we show that the electrochemical hydrogenolysis of model substrates and organosolv lignin occurs selectively on the sp^3 C—O bond, to give phenols as main products, without deterioration of the aromatic units. The electrochemical system uses stoichiometric amounts of water (H_2O) as the only hydrogen source, and inexpensive and widely available magnesium as a sacrificial electrode, to achieve a 98% phenol yield and an overall 98.8% Faradaic efficiency after optimization. Mechanistic studies based on reactive, kinetics, and isotopic experiments, among others, reveal the necessary presence in the system of tri(pyrrolidin-1-yl)phosphine oxide (TPPA) as a protecting agent against electrode passivation and lithium bromide (LiBr) as a supporting electrolyte, enabling the breaking and separation of organosolv lignin into its aromatic and alkyl organic parts. These results open the way to directly obtain the aromatic compounds present in lignin with water and electricity.

1 | Introduction

Electrochemical methods have emerged as powerful tools to drive chemical transformations under mild and tunable conditions, offering unique opportunities for selective bond activation through precise control of electron transfer [1–6]. In recent years, significant advances in synthetic organic electrochemistry have enabled a broad range of transformations, supported by improved experimental methodologies, mechanistic understanding, and practical guidance for implementation [2, 3, 7–9]. Despite these advances, electrochemical reactivity has been predominantly explored using well-defined molecular substrates, and the translation of reactivity patterns established under controlled electrochemical conditions to structurally complex and heterogeneous materials remains a major challenge [7, 8].

Among renewable feedstocks, lignin represents a particularly challenging substrate for electrochemical transformation [10–12]. As a highly irregular aromatic biopolymer composed of phenylpropanoid units linked through a diverse array of sp^3 C—O and C—C bonds, lignin exhibits substantial structural heterogeneity, broad molecular weight distributions and limited solubility [10, 11]. While numerous catalytic and thermochemical approaches (not electrochemical) have been explored for lignin depolymerization and valorization, achieving controlled and selective bond cleavage within the native lignin matrix still remains difficult [12–16]. In this context, electrochemical methods offer attractive features, such as reagent-free redox control and mild operating conditions, but their application to lignin has so far been dominated by oxidative processes or bulk electroconversion strategies, often with limited molecular-level insight [17–19]. The most precious chemical part of lignin, i.e., the phenylpropanoid units, is rarely preserved because the depolymerization reaction breaks the sp^2 bonds concomitantly with the strong sp^3 bonds to become unselective, degrading the aromatic units as well as the C—O and C—C links [12]. Indeed, electrochemical studies targeting C—O bond cleavage have largely focused on well-defined lignin model compounds, such as aryl

ether motifs, which allow systematic investigation of reaction parameters and mechanistic features [20, 21]. These studies have provided valuable insight into the feasibility of electrochemical ether cleavage and the role of electrodes, mediators, and proton sources, opening the door for a selective lignin depolymerization. However, comparatively few reports attempt to bridge the gap between reactivity observed in simple molecular models and structural modification of native lignin, and even fewer do so under carefully controlled electrochemical conditions combined with detailed experimental validation, in order to get the valuable phenylpropanoid units [17].

A critical yet underexplored question is therefore how electrochemical sp^3 C—O bond cleavage reactivity, established on model aryl ether substrates, translates to a chemically complex lignin matrix. Moreover, the question further remains for stronger sp^3 C—C bonds, also present in lignin. Motivated by this gap, we set out to explore whether simple electroreductive conditions, implemented in a commercially available electrosynthesis device (ElectraSyn 2.0, Figure S1) and employing inexpensive Mg and Zn electrodes, could promote selectively the sp^3 C—O and C—C bond hydrogenolysis under mild conditions, preserving the aromatic units. Using a robust aryl ether model substrate, we will first establish the electrochemical C—O and C—C bond hydrogenolysis under operationally simple conditions. This initial observation will then motivate us for a systematic investigation of key reaction parameters, including electrode material, solvent, electrolyte, water content, and the role of additives such as tri(pyrrolidin-1-yl)phosphine oxide (TPPA). Then, we will carry out a detailed experimental investigation of electrochemical C—O bond cleavage under constant-current conditions, combining systematic optimization of operational parameters with mechanistic control experiments. Building on this foundation, we explore the applicability of the optimized electrochemical system to organosolv lignin as a chemically demanding, heterogeneous substrate. Rather than targeting selective lignin depolymerization, our study focuses on identifying reproducible structural modifications induced by electrochemical treatment and on assessing how reactivity trends, established in model aryl ether substrates, manifest in lignin-derived fractions. Comparative nuclear magnetic resonance (NMR) analyses, among others, reveal the formation of chemically distinct lignin fractions with differing aromatic and aliphatic character, providing experimental evidence for electrochemical C—O bond cleavage chemistry to be translated, at least in part, from well-defined molecular systems to native lignin under mild conditions [22].

2 | Results and Discussion

2.1 | Initial Screening Conditions for the Electrochemical Reduction of a Model Substrate

The aryl-fused oxygen heterocycle compound **1**, rather than any commercial simpler compound, was selected as a model substrate for our electrochemical studies due to its well-defined structure, which combines an aromatic ring with a cyclic ether moiety containing different sp^3 C—O and C—C bonds, akin to lignin. Such oxygenated aromatic frameworks provide robust and synthetically accessible models for investigating the electroreductive C—O and C—C bond cleavage in complex environments, and bear conceptual relevance to lignin and related biomass-derived materials, which are rich in oxygen-containing aromatic motifs. The synthesis of compound **1** has been previously reported and can be performed on multigram scale (see Experimental Section in the Supporting Information), making it suitable for extensive optimization studies [23].

Table 1 shows the results obtained for the electrochemical reduction of compound **1** under the initial screening conditions. The reactions were performed in a nondivided cell under constant-current electrolysis using Mg as the anode, with either stainless

TABLE 1 | Results for the electrochemical reduction of model compound **1** under initial screening conditions.

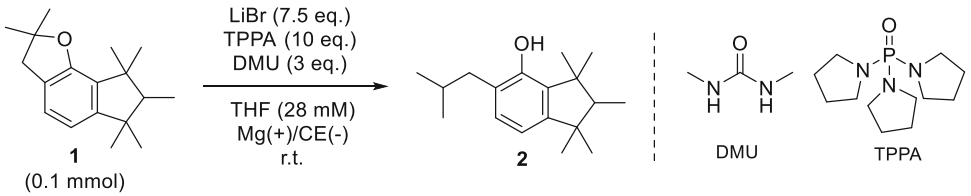

Entry	Cathode, CE	Current, mA	Charge, F/mol	Yield to 2, %	By-products[a], %
1	SS	15	9.0	7	64
2	SS	10	9.0	33	19
3	**SS**	**10**	**18.7**	**59**	**26**
4	SS	5	6.5	17	14
5	Zn	15	6.5	36	16
6	Zn	10	6.5	26	39
7	Zn	10	9.0	51	16
8	Zn	10	25.0	48	49

Note: The reactions were carried out using IKA electrodes, **1** (0.1 mmol), TPPA (10 eq.), LiBr (7.5 eq.) and 3.6 ml of THF, and double-checked after monitoring by GC–MS and ^{1}H NMR. The reactions were perfomed by duplicate, and the result given is the average.
[a]Combined yield of further hydrogenated products detected by GC and ^{1}H NMR, including species with m/z 262 and 264.

steel (SS) or Zn serving as the cathode, LiBr as a supporting electrolyte, 1,3-dimethylurea (DMU) as a proton source, tri(pyrrolidin-1-yl)phosphine oxide (TPPA) as an additive to mitigate electrode passivation, and tetrahydrofuran (THF) as a solvent. The reaction was monitored by gas chromatography (GC) combined with mass spectrometry (GC–MS) and also by proton nuclear magnetic resonance (^{1}H NMR). As summarized in Table 1, the outcome of the electrochemical reduction was found to be highly sensitive to the applied current, charge, and cathode material. Using SS as the cathode at a constant current of 10 mA, compound **1** was efficiently converted into compound **2** in 59% yield (Table 1, compare entries 1–4 and see also Figures S1–S3). High-resolution mass spectrometric analysis of the crude reaction mixture revealed two byproducts with *m/z* values of 262 and 264, alongside compound **2**. Given that the molecular weight of starting material **1** is 258, these signals are consistent with partial (+4) and full (+6) reduction of the aromatic ring, respectively (Figure S4). Although these byproducts could not be unambiguously identified, their formation highlights the presence of competing electroreductive pathways under the initial screening conditions. It must be noticed here that the reaction conditions were in principle inspired by a seminal work where aromatic ring reduction occurs [24], thus the formation of these further hydrogenated byproducts is reasonable, while the preservation of the aromatic ring in **2** must be considered remarkable. Indeed, the efficient formation of compound **2** while maintaining a moderate level of byproducts was also observed using a Zn cathode at lower charge input, affording a 51% yield of **2** (Table 1, entries 5–8). Lower currents or insufficient charge resulted in poor conversion of compound **1** (see entries 4 and 6), whereas more forcing electrochemical conditions led to increased formation of byproducts, again coming from the partial or full reduction of the aromatic ring under the strongly reducing electrochemical conditions (see entries 1 and 8). The evolution of the reaction under these forced conditions was then determined at different times, providing qualitative insight into the time-dependent formation of compound **2** and the byproducts (Figure S5), to show that the undesired second hydrogenation proceeds faster under the forced reaction conditions.

Taken together, these initial results establish that compound **1** undergoes electrochemical reduction in which sp^3 C—O but not sp^2 C—O (phenol) or C—C (including aromatic) hydrogenolysis predominates [25] while also revealing the strong dependence of product distribution on the applied electrochemical conditions. This observation prompted a systematic optimization of the reaction parameters, which is discussed in the following section.

2.2 | Optimization Study

First, the reaction was performed in the absence of TPPA, and no conversion of compound **1** was observed, highlighting the crucial role of this additive in preventing electrode passivation under the electroreductive conditions [24, 26]. Then, the role of the proton source, i.e., DMU was studied. For that, kinetic experiments were performed under constant-current, in order to assess whether changes in product distribution could be induced during the reaction. Thus, the electrochemical reaction was performed from the beginning without DMU, and the formation of compound **2** was still observed, although with a slower overall reaction rate and an apparent induction period (Figure S6). This result seems to indicate that DMU is not necessary for product **2** to be formed. Indeed, when the reaction was carried out in the presence of DMU (Mg(+)/SS(–), 10 mA, 25 F/mol), interrupted after partial conversion, subjected to standard work-up to remove additives, and then resumed in the presence of TPPA but in the absence of DMU, the electrohydrogenolysis proceeded further and resulted in a continued increase in the yield of compound **2** (Figure S7). This experiment confirms that the use of DMU is not required for the formation of product **2** and that, in the absence of DMU, the reaction proceeds with high selectivity toward the desired product **2**. This led us to investigate the actual proton source responsible for the sp^3 C—O bond breaking process.

Given that DMU was not required for product formation, Karl–Fischer titration of the individual reaction components were carried out to determine the presence of residual water in the reaction medium, with LiBr and TPPA identified as the major contributors (Figure S8 and Table S1). The amount of residual water in the 'dry' system, thus twice hydrogen atoms, is approximately one equivalent respect to **1**, enough to sustain the hydrogenation reaction quantitatively [27]. This observation suggests that trace amounts of water present in the reaction mixture could act as the effective proton source during the electrochemical reduction. Under these DMU-free reaction conditions, a comparative evaluation of different electrodes revealed that the Mg(+)/Zn(–) combination provided the most efficient formation of compound **2**, affording yields of up to 89.9% (Table S2). On this basis, this electrode pair was selected to evaluate the influence of water content under controlled reaction conditions. The reactions were performed using dry THF while varying the amount of added water. As summarized in Table 2, efficient formation of compound **2** was achieved with low amounts of water, particularly when dry THF was employed, to achieve a remarkable 90% of **2** with 94% selectivity (entry 3). While the reaction tolerated

TABLE 2 | Results for the electrochemical reduction of model compound **1** with different amounts of H_2O.

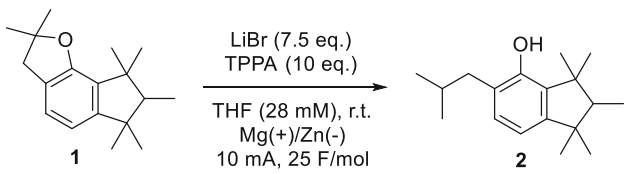

Entry	Dry THF	Additional H_2O, eq.	Yield to 2, %	Byproducts, %
1	No	0	64.0	2.4
2	No	1	71.6	6.7
3	**Yes**	**0**	**90.0**	**5.8**
4	Yes	1	84.7	10.2
5	Yes	3	69.2	16.5

Note: The reactions were carried out using IKA electrodes Mg(+)/Zn(–), **1** (0.1 mmol), TPPA (10 eq.), LiBr (7.5 eq.), and 3.6 mL of THF. With dry reactants/solvent, the amount of residual water is approximately 1 equivalent to complete the hydrogenolysis reaction. The reactions were set up at 10 mA (constant current) and 25 F/mol, and double-checked after monitoring by GC–MS and ^{1}H NMR. The reactions were perfomed by duplicate, and the result given is the average.

small amounts of added water, higher water loadings led to reduced selectivity for **2**. This trend is consistent with kinetics experiments performed using dry and nondry LiBr, in which the use of dried LiBr resulted in an approximately 10% higher yield of compound **2** compared to LiBr used as received (Figure S9). Karl–Fischer analysis indicated that the water content associated with nondried LiBr corresponds approximately to one equivalent of water relative to compound **1**, in good agreement with the decrease in yield observed upon intentional addition of one additional equivalent of water (Table 2, entries 3 and 4). Overall, these studies indicate that excess proton availability favors competing electroreductive pathways, resulting in reduced selectivity toward C—O bond hydrogenolysis and, in some cases, premature termination of electrolysis due to a rapid increase in cell potential [28].

The effect of the solvent and electrolyte was briefly examined under the new optimized electrochemical conditions. Using the Mg(+)/Zn(−) electrode pair, several commonly used solvents for reductive electrosynthesis, such as MeCN, DMF, and DMSO, were screened. In contrast to THF, which consistently afforded efficient formation of compound **2**, the use of these solvents resulted in negligible formation of **2** (<1%), often accompanied by increased cell potential or electrode passivation (Table S3). It must be noted here that the breaking of THF solvent bonds by Mg metal was not observed, although it cannot be discarded [29]. Regarding the electrolyte, other lithium halide salts such as LiI were found to be suitable for this transformation, affording comparable yields of compound **2** than LiBr (Table S4) [30]. In contrast, other electrolytes such as NaCl, NaBr, $NaBF_4$, and NH_4Br showed insufficient solubility in THF and were therefore not considered.

The role of TPPA was subsequently examined under the optimized solvent and electrolyte conditions, and, again, it was found to be essential to sustain productive electrolysis, as when DMU was present in the reaction medium. Decreasing the amount of TPPA led to a pronounced decrease in reaction efficiency, while the absence of TPPA resulted in complete suppression of product formation, consistent with rapid electrode passivation under the electroreductive conditions (Table S5). These results indicate that TPPA plays a critical operational role in maintaining electrode activity throughout the electrolysis, either with or without DMU. Attempts to replace TPPA with alternative additives were unsuccessful, in particular, the use of triphenylphosphine oxide (TPPO) did not result in detectable formation of compound **2**. ^{31}P NMR monitoring experiments, in which TPPA and TPPO were simultaneously present in the reaction mixture (Figure S10), showed that TPPA remained largely intact during the reaction, exhibiting only minor degradation (≤10%), whereas TPPO underwent significant degradation under the same reaction conditions [31]. The higher stability of TPPA may be related to the electronic nature of the substituents at the phosphorus atom [32].

The combined influence of substrate concentration and applied current on the electrochemical reduction of compound **1** was next examined. Preliminary experiments conducted at a substrate concentration of 25 mM and varying the applied current in the presence of one equivalent of added water revealed that increasing the current to 15–20 mA led to a rapid rise in cell potential, in some cases reaching the voltage limit of the instrument (Table S6). This behavior was not observed when the substrate concentration was increased. As illustrated in Figure 1 (see also Table S7), increasing the substrate concentration from 25 to 50 mM at a constant current of 10 mA resulted in a slower formation of compound **2** while maintaining comparable final yields (≈84%) at a given charge input. Notably, higher substrate concentration enabled the application of increased current without compromising the stability of the electrochemical system. At 50 mM of **1**, increasing the current from 10 to 15 mA led to higher yields of compound **2**, to finally achieve a remarkable 98%. Besides, not only the final yield but also the initial rate increases with substrate concentration (Figure S11). These effects are consistent with a reduced availability of electroactive substrate at the electrode surface under conditions of high proton availability or low substrate concentration, which can lead to inefficient consumption of the applied current, manifested as reduced selectivity

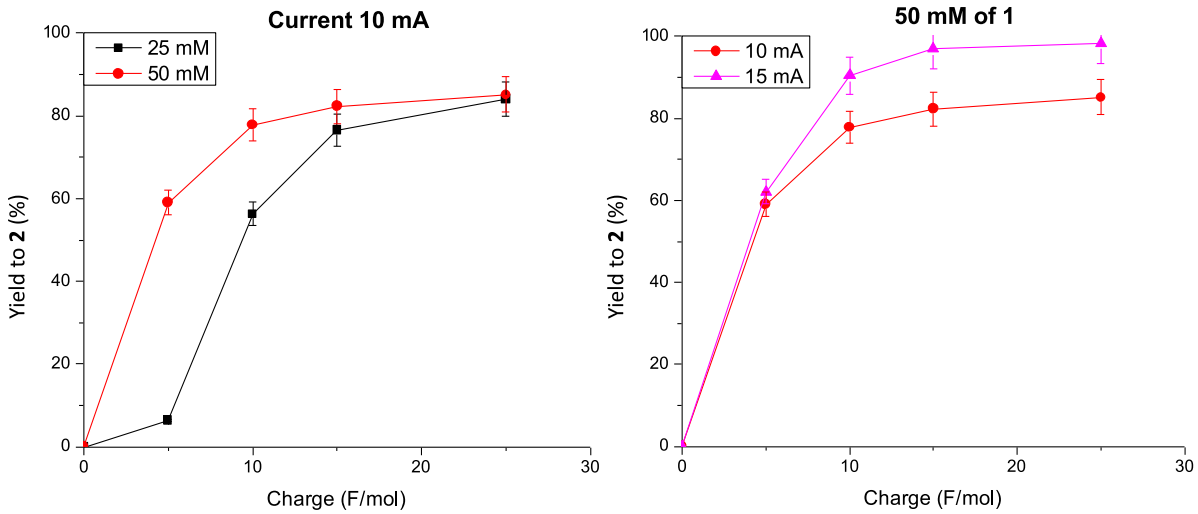

FIGURE 1 | Effect of substrate concentration and applied current on the electrochemical reduction of compound **1**. Reactions were performed in an undivided cell using Mg(+)/Zn(−) electrodes, TPPA (10 eq.), LiBr (7.5 eq.), and dry THF (4 mL). Formation of compound **2** as a function of charge under left) different substrate concentrations (25 and 50 mM) at a constant current of 10 mA, and right) different applied currents (10 and 15 mA) at a substrate concentration of 50 mM. Error bars account for a 5% uncertainty.

toward compound **2** and/or an increase in cell potential. Overall, these results indicate that substrate concentration and applied current must be carefully balanced to maintain a stable electrochemical regime and achieve efficient and selective sp^3 C—O bond hydrogenolysis under the present conditions [33].

2.3 | Mechanistic Considerations

Several experiments were then performed to gain insight into the nature of the electrochemical transformation. First, a kinetic experiment in which the current was stopped at 5 F/mol during product formation showed that the formation of **2** was strictly dependent on the electrical current because no further formation of compound **2** was observed when the current was interrupted at approximately 55% conversion (Figure S12). This result unambiguously indicates that the reaction does not proceed via a purely chemical pathway.

Isotopic labeling experiments provided direct evidence regarding the origin of the protons involved in the ring-opening process. When the reaction was conducted in the presence of D_2O, deuterium incorporation was observed in the aliphatic fragment of the ring-opened product (Figure S13–S14) [34]. Notably, deuterium incorporation was not detected at the phenolic O—H position, which is likely due to rapid H/D exchange with residual protic species present in the reaction medium or during work-up. In contrast, no deuterium incorporation was observed when the reaction was performed in THF–d^8. These results, together with the sensitivity of the reaction to proton availability, identify water as the effective proton source during electrochemical C—O bond hydrogenolysis and suggest that controlled proton delivery is a key factor governing selectivity and electrochemical stability [8].

In electrochemical reductive transformations, metals such as Mg are commonly employed as sacrificial anodes, as they readily undergo anodic dissolution while enabling electron delivery to the cathodic process [35]. In this context, the role of the Mg electrode was examined in more detail. Reactions conducted using new or reused Mg anodes afforded comparable reaction profiles and final yields (Figure S15), indicating that gradual electrode consumption does not adversely affect reaction efficiency. Consistent with this behavior, gravimetric analysis revealed a mass loss of approximately 60 mg (2.47 mmol) of Mg per reaction at a charge input of 25 F/mol. Assuming anodic oxidation of Mg to Mg^{2+}, this mass loss corresponds approximately to 4.94 mmol of electrons, which closely matches the total charge passed (25 F/mol × 0.2 mmol of substrate = 5.0 mmol electrons), in agreement with magnesium acting as a sacrificial anode under the electroreductive conditions. These numbers give a Faradaic efficiency (FE) of 98.8% for the whole process.

Additional insights were obtained from electrode-switching experiments. When the Mg anode was replaced by a Zn electrode after partial conversion (≈25%), electrolysis could be resumed and product formation continued, although at a slower rate compared to uninterrupted reaction with the Mg anode (Figure S16). In contrast, reactions conducted exclusively with Zn electrodes were ineffective (see Table S2). These observations suggest that metallic Mg plays a critical role during the initial stages of the electrochemical transformation, while continued electron flow can sustain product formation once the process has been initiated.

To further probe the role of Mg in the electrochemical transformation, a series of control experiments was performed using different additives (Table S8). When the reaction was conducted using Zn(+)/Zn(−) electrodes in the presence of metallic Mg turnings, productive electrolysis was observed even in the absence of a Mg anode. In contrast, the use of soluble Mg salts (MgI_2, $MgBr_2$, $MgCl_2$) did not promote product formation and, in several cases, led to rapid electrode passivation, even when a Mg anode was present (Figure S17) [36]. Additional experiments showed that neither metallic Zn nor $AlCl_3$ reproduced the effect of Mg, and the presence of a crown ether, as a complexing agent, did not significantly alter the reaction outcome. Together, these observations indicate that the presence of metallic Mg, rather than dissolved Mg species or simple Lewis acidic additives, is required to sustain productive electrolysis under the reaction conditions [37]. It must be said here that cyclic voltammetry (CV) experiments were conducted to gain qualitative insight into the electrochemical behavior of the reaction components but, under the reaction conditions, the voltammetric response was dominated by TPPA, which is present in excess and exhibits electroactivity within the explored potential window (Figure S18). As a result, no distinct electrochemical features attributable to compound **1** or product **2** could be reliably identified. Consequently, the CV data could not be used to derive mechanistic conclusions.

Taken together, these observations support the reaction scenario shown in Figure 2, in which electrochemical sp^3 C—O bond hydrogenolysis is governed by controlled electron flow, regulated proton availability, and the presence of metallic Mg in solution [38] under conditions that maintain an active electrode surface.

2.4 | Reactivity of Other Aryl ether Substrates and Application to Lignin Depolymerization

To further explore the reactivity of the electrochemical system beyond the model substrate, a small set of additional aryl ether compounds was evaluated under the optimized conditions (Figure S19). Simple aryl alkyl ethers, such as anisole and benzodioxole, underwent efficient sp^3 C—O bond cleavage to afford the corresponding phenols in high yields, without any breaking of the sp^2 C—O phenol bond. Substrates bearing additional functional groups or extended conjugation, including alkynes or chromanone derivatives, resulted in competing reduction pathways [39], nevertheless, keeping untouched the phenol ring products. Only when catechol-derived substrates were employed as

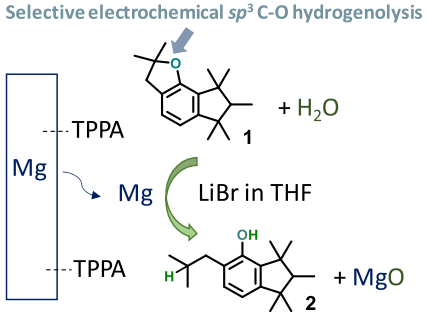

FIGURE 2 | Proposed reaction pathway for the electrochemical hydrogenolysis of aryl ether **1** to phenol **2** under the optimized reaction conditions.

reactants, the breaking of one of the sp^2 C—O bonds was observed, keeping the other one intact, to give a phenol as a final product. These results highlight the high selectivity of the electroreductive reaction to form phenols as final products, despite the expected pronounced sensitivity of the electrochemical transformation to substrate structure and electronic properties. The observed reactivity trends are consistent with the ability of our electroreductive system to promote alkyl vs aryl C—O bond cleavage in aromatic substrates.

Encouraged by the observed electrochemical C—O bond hydrogenolysis in a well-defined model substrate and related aryl ethers, we next explored the applicability of the optimized electroreductive conditions to a more complex and structurally heterogeneous material, such as organosolv lignin, shown in Figure 3 [40]. Electrochemical treatment of organosolv lignin was evaluated under several sets of conditions, varying the amount of lignin, the applied current, and the cathode material (see also Table S9). All experiments were performed in an undivided cell using an IKA ElectraSyn setup equipped with a Mg sacrificial anode under constant-current electrolysis. After work-up, complex reaction mixtures were obtained, consistent with the structural heterogeneity of lignin. Multiple ^{1}H and ^{13}C{^{1}H} NMR datasets were collected across experiments, and the discussion below focuses on representative spectra that capture the main qualitative features observed upon electrochemical treatment.

After electrolysis and chromatographic work-up on silica, two operationally distinct fractions were obtained: (i) a nonretained soluble fraction that readily eluted through silica, and (ii) a fraction initially retained on silica, which could be recovered upon elution with a more polar solvent. Figure 4 compares the ^{1}H NMR spectra of these fractions with that of the starting lignin. First, a clear qualitative change not only in the ^{1}H NMR spectrum relative to the starting material but also in the corresponding ^{13}C{^{1}H} NMR spectra (Figures S20–S23) can be observed, including the emergence of new signals consistent with phenolic and carbonyl-containing functionalities as well as a redistribution of signals in the aromatic and aliphatic regions. Notably, the silica-retained fraction displays a higher relative contribution of aromatic signals in both the ^{1}H (6–8 ppm) and ^{13}C{^{1}H} (110–160 ppm) NMR spectra, consistent with highly functionalized, polar aromatic lignin-derived materials [41, 42]. The signal for the phenol protons at 6.0 ppm is clearly observed. In addition, other signals clearly visible in the 9–10 ppm region of the ^{1}H NMR spectra of this retained fraction are consistent with aldehydic protons, suggestive of aromatic or conjugated aldehyde motifs associated with highly functionalized lignin-derived structures. These species come from the dehydrogenation of benzyl alcohol products, also expected after the breaking of lignin [43]. This interpretation is further supported by the appearance of carbonyl signals around 195 ppm in the corresponding ^{13}C{^{1}H} NMR spectra. Accordingly, aldehyde-containing aromatic motifs are included as representative structures in the reaction scheme shown in Figure 3. The absence of well-defined vinyl proton signals and the lack of signals in the ^{13}C{^{1}H} NMR spectra in the 126–130 ppm range suggest that α,β-unsaturated aldehyde motifs are not predominant, and that the observed aldehydic signals are more consistent with aromatic aldehyde functionalities. Fourier-transform infrared (FT-IR) characterization confirms the enrichment of this product fraction in phenol-derived aromatic products (in average mass) compared to the starting organosolv lignin after a clear increase in the signals in the 1600–1700 cm^{-1} area (Figure S24). Tentative assignments of selected ^{1}H and ^{13}C{^{1}H} NMR signals supporting the representative lignin-derived motifs depicted in Figure 3 are also provided in the Supporting Information (Figure S25) [44].

In contrast, the nonretained soluble fraction shows a marked predominance of aliphatic and oxygenated aliphatic signals with only minor aromatic contributions observable upon signal expansion, not only by NMR (Figure S26) bus also by FT-IR (increase in the signals around 1200 cm^{-1}, Figure S24). Tentative aliphatic and carbonyl-containing lignin-derived motifs consistent with this fraction are proposed in Figure 3, and further reproductions of the electrochemical reaction under slightly different conditions led to

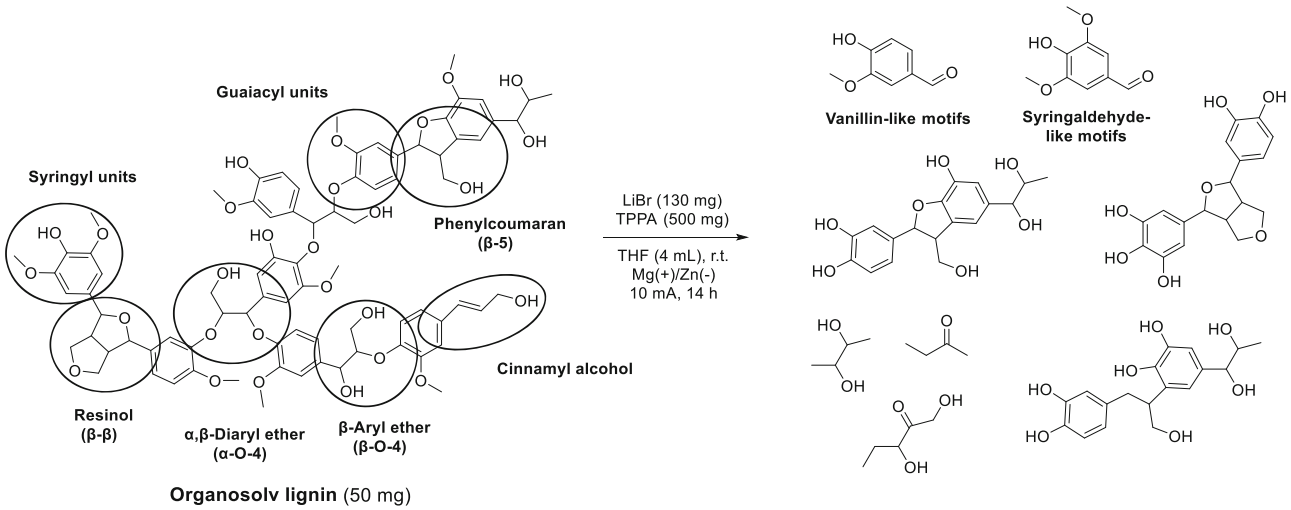

FIGURE 3 | Main products found during the electrochemical reaction of organosolv lignin. A representative structural motif commonly attributed to organosolv lignin is shown. The reaction was carried out in an undivided cell using an IKA ElectraSyn setup equipped with Mg(+)/Zn(–) electrodes. An ElectraSyn vial was charged with lignin organosolv (50 mg), TPPA (500 mg), LiBr (130 mg), and dry THF (4 mL), followed by constant-current electrolysis at 10 mA. The reactions were perfomed by duplicate, and the result given is the average. The tentative lignin-derived aromatic structures are shown for illustrative purposes.

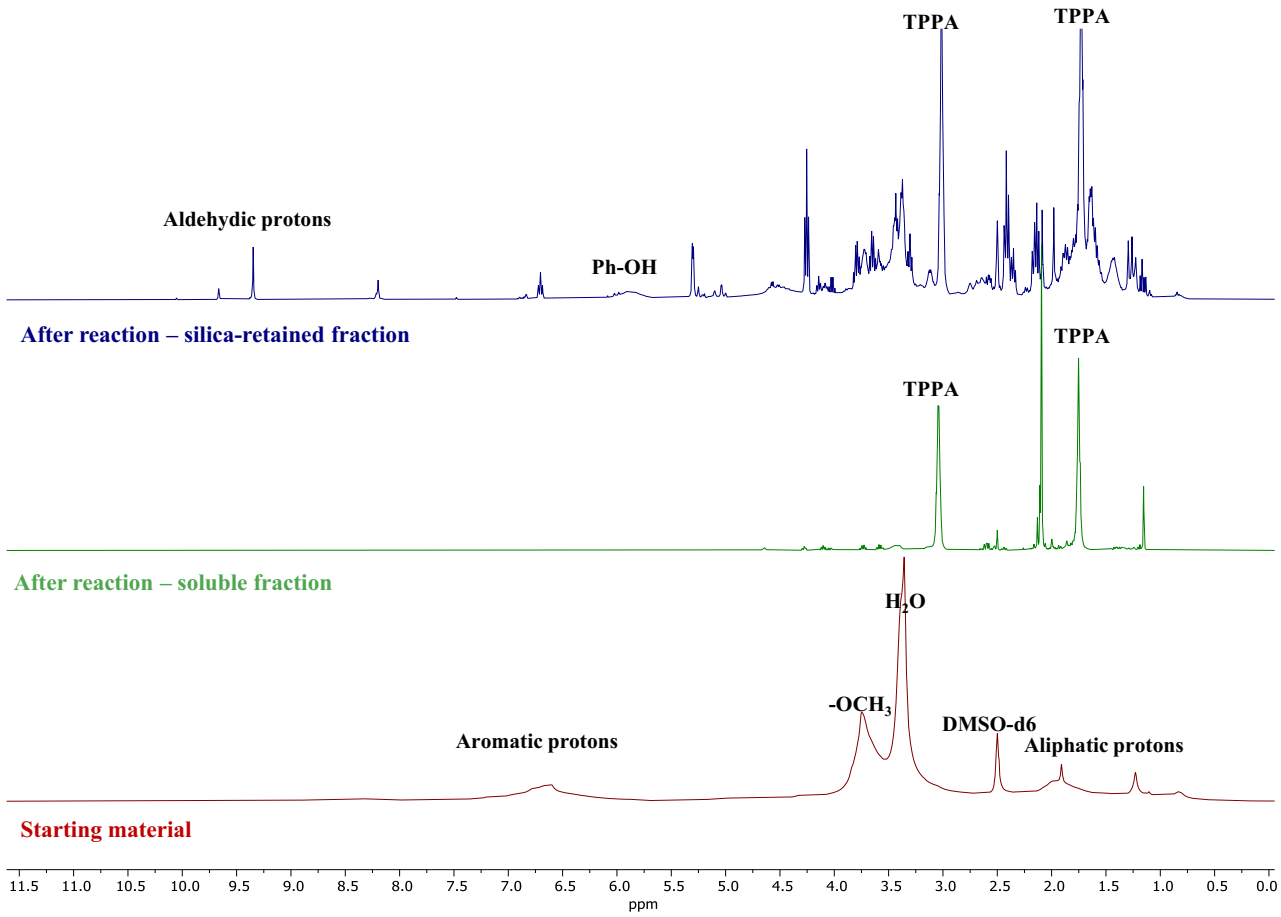

FIGURE 4 | Comparison of the ^{1}H NMR spectra (DMSO–d_6) of organosolv lignin before and after electrochemical treatment. From top to bottom: (blue) silica-retained fraction (initially retained on silica and subsequently eluted with additional/more polar solvent), (green) nonretained soluble fraction (eluate after passage through silica), and (red) starting organosolv lignin. Reaction conditions in Table S9, entry 1.

similar results (Figures S27–S29). This spectroscopic differentiation indicates that the electrochemical treatment leads to the expected formation of the chemically distinct lignin-derived fractions, one containing the aromatic units (silica-retained fraction) and another the alkyl containing fraction (nonretained fraction), after sp^3 C—O (and perhaps also sp^3 C—C) bond breaking [45], without any observation of aromatic degradation after complete consumption of the starting organosolv lignin [46]. These results with lignin are in good agreement with the studies above with model substrates, and showcase the possibility of separating the aromatic from the alkyl fraction in the original lignin after the electrochemical treatment [47]. It is noteworthy to comment that the stability of the depolymerized lignin product mixture is also relevant because several electrochemical by-reactions might also occur [48–50].

3 | Conclusion

The electroreduction not only of model substrates but also of organosolv lignin occurs, after optimization, in high yield toward the phenol products (up to 98%) and high overall FE (98.8%) with minimal amounts of water. The efficiency of the electrochemical system is based on the use of Mg as a sacrificial electrode, to selectively break the sp^3 C—O bonds present in lignin and substrate models but not other C—O or C—C bonds [51, 52]. This valorization of lignin into aromatic products employs inexpensive materials and enables the easy separation of the aromatic and alkyl constituents in organosolv lignin, providing a straightforward way to directly obtain the individual organic compounds. Mechanistic studies, involving kinetic and isotopic experiments among others, reveal the necessary presence in the system of tri(pyrrolidin-1-yl)phosphine oxide (TPPA) as a protecting agent against passivation and lithium bromide (LiBr) as a supporting electrolyte. Given that lignin valorization is one of the main current challenges in chemistry [53–56], involving different fields such as synthetic chemistry, catalysis and sustainable chemistry, the results here shown can open new directions in the field [57, 58].

Acknowledgments

This work was part of the project PID2023-148441NB-I00 financed by MICIIN, and financial support by project CPP2022-009991 and the Severo Ochoa Centre of Excellence program (CEX2021-001230-S) is gratefully acknowledged. M. M.-G. thanks ITQ, UPV-CSIC, for the concession of a contract (PAID 01-23).

Funding

This work was supported by the Ministerio de Ciencia e Innovación (PID2023-148441NB-I00, CPP2022-009991, CEX2021-001230-S); Universitat Politècnica de València (PAID 01-23).

Conflicts of Interest

The authors declare no conflicts of interest.

Data Availability Statement

The data that support the findings of this study are available from the corresponding author upon reasonable request.

References

1. A. Wiebe, T. Gieshoff, S. Möhle, E. Rodrigo, M. Zirbes, and S. R. Waldvogel, "Electrifying Organic Synthesis," *Angewandte Chemie International Edition* 57 (2018): 5594–5619.

2. M. Yan, Y. Kawamata, and P. S. Baran, "Synthetic Organic Electrochemical Methods Since 2000: On the Verge of a Renaissance," *Chemical Reviews* 117 (2017): 13230–13319.

3. K. D. Moeller, "Using Physical Organic Chemistry to Shape the Course of Electrochemical Reactions," *Chemical Reviews* 118 (2018): 4817–4833.

4. C. Costentin and J.–M. Savéant, "Towards an Intelligent Design of Molecular Electrocatalysts," *Nature Reviews Chemistry* 1 (2017): 0087.

5. S. R. Waldvogel and B. Janza, "Renaissance of Electrosynthetic Methods for the Construction of Complex Molecules Angew," *Angewandte Chemie International Edition* 53 (2014): 7122–7123.

6. F. He, Y. Wang, X. Huang, S. Qu, and J. Liu, "Photo– and Electro–Chemical Strategies for the Activation of Strong Chemical Bonds," *Chemical Society Reviews* 53 (2024): 263–316.

7. C. Kingston, M. D. Palkowitz, Y. Takahira, et al., "A Survival Guide for the "Electro–curious," *Accounts of Chemical Research* 53 (2020): 72–83.

8. S. Möhle, M. Zirbes, E. Rodrigo, T. Gieshoff, A. Wiebe, and S. R. Waldvogel, "Modern Electrochemical Aspects for the Synthesis of Value–Added Organic Products Angew," *Angewandte Chemie International Edition* 57 (2018): 6018–6041.

9. J.–I. Yoshida, K. Kataoka, R. Horcajada, and A. Nagaki, "Modern Strategies in Electroorganic Synthesis," *Chemical Reviews* 108 (2008): 2265–2299.

10. A. J. Ragauskas, G. T. Beckham, M. J. Biddy, et al., "Lignin Valorization: Improving Lignin Processing in the Biorefinery," *Science (new York, N.y.)* 344 (2014): 1246843.

11. J. Ralph, C. Lapierre, and W. Boerjan, "Lignin Structure and Its Engineering," *Current Opinion in Biotechnology* 56 (2019): 240–249.

12. C. Li, X. Zhao, A. Wang, G. W. Huber, and T. Zhang, "Catalytic Transformation of Lignin for the Production of Chemicals and Fuels," *Chemical Reviews* 115 (2015): 11559–11624.

13. Z. Sun, B. Fridrich, A. de Santi, S. Elangovan, and K. Barta, "Bright Side of Lignin Depolymerization: Toward New Platform Chemicals," *Chemical reviews* 118, no. 2 (2018): 614–678.

14. C. Yang, J. Qin, S. Sun, et al., "Progress in Developing Methods for Lignin Depolymerization and Elucidating the Associated Mechanisms," *European Polymer Journal* 210 (2024): 112995.

15. J. Kim, C. Kim, C. Jeong, et al., "Integrated Process for Lignin Depolymerization and Nanoparticle Production Using Deep Eutectic Solvent," *Scientific Reports* 15 (2025): 11770.

16. J. Zakzeski, P. C. A. Bruijnincx, A. L. Jongerius, and B. M. Weckhuysen, "The Catalytic Valorization of Lignin for the Production of Renewable Chemicals," *Chemical Reviews* 110 (2010): 3552–3599.

17. M. García–Rollán, M. Toscano–de los Riscos, R. Ruiz–Rosas, J. M. Rosas, J. Rodríguez–Mirasol, and T. Cordero, "Oxidative Electrochemical Depolymerization of Lignin Using Highly Active Self–Standing Electrocatalysts Prepared by Electrospinning of Lignin," *Biomass & Bioenergy* 193 (2025): 107560.

18. B. A. Frontana–Uribe, R. D. Little, J. G. Ibañez, A. Palma, and R. Vasquez–Medrano, "Organic Electrosynthesis: A Promising Green Methodology in Organic Chemistry," *Green Chemistry* 12 (2010): 2099–2119.

19. B. Huang, Z. Sun, and G. Sun, "Recent Progress in Cathodic Reduction–Enabled Organic Electrosynthesis: Trends, Challenges, and Opportunities," *eScience* 2 (2022): 243–277.

20. C. Yang, G. Magallanes, S. Maldonado, and C. R. J. Stephenson, "Electro–Reductive Fragmentation of Oxidized Lignin Models," *The Journal of Organic Chemistry* 86 (2021): 15927–15934.

21. F. He, Y. Wang, X. Huang, S. Qu, and J. Liu, "Electrochemical C–*O* Bond Cleavage of Diaryl Ethers: Upcycling of Lignin 4–O–5 Models and Polyphenylene Oxide," *Green Chemistry* 27 (2025): 9178–9186.

22. X. Du, H. Zhang, K. P. Sullivan, P. Gogoi, and Y. Deng, "Electrochemical Lignin Conversion," *ChemSusChem* 13 (2020): 4318–4343.

23. F. Garnes–Portolés, S. Sanz–Navarro, J. Ballesteros–Soberanas, et al., "Indomuscone–Based Sterically Encumbered Phosphines as Ligands for Palladium–Catalyzed Reactions," *The Journal of Organic Chemistry* 88, no. 9 (2023): 5962–5971.

24. B. K. Peters, K. X. Rodriguez, S. H. Reisberg, et al., "Scalable and Safe Synthetic Organic Electroreduction Inspired by Li–Ion Battery Chemistry," *Science (new York, N.y.)* 363 (2019): 838–845.

25. W.–B. Wu and J.–M. Huang, "Electrochemical Cleavage of Aryl Ethers Promoted by Sodium Borohydride," *The Journal of Organic Chemistry* 79 (2014): 10189–10195.

26. M. Ishifune, H. Yamashita, Y. Kera, et al., "Electroreduction of Aromatics Using Magnesium Electrodes in Aprotic Solvents Containing Alcoholic Proton Donors," *Electrochimica Acta* 48 (2003): 2405–2409.

27. M. Mon and A. Leyva–Pérez, "Industrial Synthesis of Allyl Alcohols: Outlook and Challenges for a Sustainable Production," *ACS Sustainable Chemistry & Engineering* 13 (2025): 19916–19936.

28. K. S. Westendorff, M. J. Hülsey, T. S. Wesley, Y. Román–Leshkov, and Y. Surendranath, "Electrically Driven Proton Transfer Promotes Brønsted Acid Catalysis by Orders of Magnitude," *Science (new York, N.y.)* 383 (2024): 757–763.

29. E. Bartmann, "Ether Cleavage by Activated Metals I. Cleavage if Tetrahydrofuran By Transition–Metal Activated Magnesium," *Journal of Organometallic Chemistry* 284 (1985): 149–158.

30. M. Espinosa, M. Molina–García, D. Ciscares–Velázquez, and A. Leyva–Pérez, "Countercation– and Solvent–Controlled Selective Borohydride Hydrogenation of Alkenes in Diaryl Enones," *Organic Chemistry Frontiers* 12 (2025): 4708–4721.

31. B. Lerma–Berlanga and A. Leyva–Pérez, "The Reductive Addition–Oxidative Elimination Mechanism," *ChemistryEurope* (2025): e202400086.

32. J. Ballesteros–Soberanas and A. Leyva–Pérez, "Electron–Poor Phosphines Enable the Selective Semihydrogenation Reaction of Alkynes with Pd on Carbon Catalysts," *The Journal of Physical Chemistry Letters* 14 (2023): 965–970.

33. Y. Zhong, Z. Ouyang, J. Wang, et al., "Ultraselective C—O Hydrogenolysis of Biomass–Based Compounds under Ambient Pressure and at Low Temperature via Hydrogen Spillover over the Pd–SO_4^{2-} Interface," *ACS Catalysis* 15 (2025): 10018–10029.

34. F. Bu, Y. Deng, J. Xu, et al., "Electrocatalytic Reductive Deuteration of Arenes and Heteroarenes," *Nature* 634 (2024): 592–599.

35. Y. Li, L. Wen, and W. Guo, "A Guide to Organic Electroreduction Using Sacrificial Anodes," *Chemical Society Reviews* 52 (2023): 1168–1188.

36. K. S. Lee and K. D. Kim, "A Convenient and Efficient Method for Demethylation of Aryl Methyl Ethers with Magnesium Iodide in Ionic Liquid," *Bulletin of the Korean Chemical Society* 31 (2010): 3842–3843.

37. L. Cardinale, G. L. Beutner, C. Y. Bemis, D. J. Weix, and S. S. Stahl, "Non–Innocent Role of Sacrificial Anodes in Electrochemical Nickel–Catalyzed $C(sp^2)$–$C(sp^3)$ Cross–Electrophile Coupling," *Journal of the American Chemical Society* 146 (2024): 32249–32254.

38. C. Kuai, L. Liu, A. Hu, et al., "Dissolved Fe Species Enable a Cooperative Solid–molecular Mechanism for the Oxygen Evolution Reaction on NiFe–based Catalysts," *Nature Catalysis* 8 (2025): 523–535.

39. J. T. Kleinhaus, J. Wolf, K. Pellumbi, et al., "Developing Electrochemical Hydrogenation towards Industrial Application," *Chemical Society Reviews* 52 (2023): 7305–7332.

40. C. Inkrod, M. Raita, V. Champreda, and N. Laosiripojana, "Characteristics of Lignin Extracted from Different Lignocellulosic Materials via Organosolv Fractionation," *BioEnergy Research* 11 (2018): 277–290.

41. J. Ralph and L. L. Landucci, *NMR of Lignins in Lignin and Lignans: Advances in Chemistry*, (CRC Press, 2010), 137–244.

42. J. C. del Río, J. Rencoret, P. Prinsen, Á.T. Martínez, J. Ralph, and A. Gutierrez, "Structural Characterization of Wheat Straw Lignin by NMR," *Journal of Agricultural and Food Chemistry* 60 (2012): 5922–5935.

43. R. Shi, X. Zhang, C. Li, et al., "Electrochemical Oxidation of Concentrated Benzyl Alcohol to High–Purity Benzaldehyde via Superwetting Organic–Solid–Water Interfaces," *Science Advances* 10 (2024): eadn0947.

44. C.–Y. Ma, Y. Xu, L.–H. Xu, C. Zhang, J.–Y. Qi, and J.–L. Wen, NMR Characterization of Lignin, eds Y. Liao, and B. F. Sels, (Wiley, 2024), 15–60.

45. A. Rahimi, A. Ulbrich, J. J. Coon, and S. S. Stahl, "Formic–Acid–Induced Depolymerization of Oxidized Lignin to Aromatics," *Nature* 515 (2014): 249–252.

46. P. Hu, B. K. Peters, C. A. Malapit, et al., "Electroreductive Olefin−Ketone Coupling," *Journal of the American Chemical Society* 142 (2020): 20979–20986.

47. S. Dong and G. Feng, "A Comprehensive Review of Catalytic Hydrodeoxygenation of Lignin–Derived Phenolics to Aromatics," *Molecules (basel, Switzerland)* 30 (2025): 2225.

48. C. Zhu, N. W. J. Ang, T. H. Meyer, Y. Qiu, and L. Ackermann, "Organic Electrochemistry: Molecular Syntheses with Potential," *ACS Central Science* 7 (2021): 415–431.

49. H. Huang and T. H. Lambert, "Electrophotocatalytic C–H Heterofunctionalization of Arenes," *Angewandte Chemie International Edition* 60 (2021): 11163–11167.

50. H. Zhu, M. Cai, X. Wang, and L. Dai, "Highly Efficient Electro–Epoxidation of Olefins Coupled with Bromine Recycling," *Green Chemistry* 27 (2025): 5366–5375.

51. A. G. Sergeev and J. F. Hartwig," Selective, Nickel–Catalyzed Hydrogenolysis of Aryl Ethers,"*Science* 332 (2011): 439–443.

52. R. Wu, Q. Meng, J. Yan, et al., "Intermetallic Synergy in Platinum–Cobalt Electrocatalysts for Selective C–O Bond Cleavage," *Nature Catalysis* 7 (2024): 702–718.

53. H. Wang, Y. Zhao, Z. Ke, et al., "Synthesis of Renewable Acetic Acid from CO_2 and Lignin over an Ionic Liquid–Based Catalytic System," *Chemical Communications* 55 (2019): 3069–3072.

54. X. Shen, Q. Meng, M. Dong, et al., "Low–Temperature Reverse Water–Gas Shift Process and Transformation of Renewable Carbon Resources to Value– Added Chemicals," *ChemSusChem* 12 (2019): 5149–5156.

55. R.–G. Hu, Y. Sang, F.–F. Tan, Y.–L. Sun, X.–S. Xue, and Y. Li, "Photoredox and Vanadate Cocatalyzed Hydrolysis of Aryl Ethers at Ambient Temperature," *ACS Catalysis* 13 (2023): 9264–9273.

56. X. Zhao, C. Li, J. Wen, et al., "Catalytic Refining Lignin into Toluene over Atomically Dispersed Cu/Ni Dual Sites," *Nature Communications* 16 (2025): 7967.

57. Y. P. Wijaya, K. J. Smith, C. S. Kim, and E. L. Gyenge, "Electrocatalytic Hydrogenation and Depolymerization Pathways for Lignin Valorization: Toward Mild Synthesis of Chemicals and Fuels from Biomass," *Green Chemistry* 22 (2020): 7233–7264.

58. M. Huddleston and Y. Sun, "Biomass Valorization via Paired Electrocatalysis," *ChemSusChem* 18 (2025): e202402161.

Supporting Information

Additional supporting information can be found online in the Supporting Information section. The experimental section, additional Figures S1–S29, Tables S1–S9 and compound characterization can be found in the Supporting Information. **Supporting Fig. S1**: Typical reaction set-up for the electrochemical reactions in the IKA Electrasyn 2.0. **Supporting Fig. S2**: Mass chromatography spectra of the model substrate **1**. **Supporting Fig. S3**: Mass chromatography spectra of compound **2**, as the major product observed under the electroreductive conditions. **Supporting Fig. S4**: Mass chromatography spectra of the two further hydrogenated byproducts. **Supporting Fig. S5**: Kinetics of the electrochemical reduction of compound **1**, in the presence of DMU. Reactions were carried out in an undivided cell using an IKA ElectraSyn setup equipped with Mg(+)/SS(–) electrodes. An ElectraSyn vial was charged with compound **1** (0.4 mmol), TPPA (10 eq.), LiBr (7.5 eq.), DMU (3 eq.) and dry THF (14.4 mL), followed by constant-current electrolysis at 10 mA to a total charge of 25 F/mol. Error bars account for a 5% uncertainty. **Supporting Fig. S6**: Kinetics of the electrochemical reduction of compound **1** without DMU as a source of protons. Reactions were carried out in an undivided cell using an IKA ElectraSyn setup equipped with Mg(+)/SS(–) electrodes. The ElectraSyn vial was charged with compound 1 (0.4 mmol), TPPA (10 eq.), LiBr (7.5 eq.), and THF (14.4 mL), followed by constant-current electrolysis at 10 mA to a total charge of 25 F/mol. An induction time can be seen before our desired product 2 starts forming without other byproducts. Error bars account for a 5% uncertainty. **Supporting Fig. S7**: Kinetics of the electrochemical reduction of compound **1** with removal of DMU during the reaction. Reactions were carried out in an undivided cell using an IKA ElectraSyn setup equipped with Mg(+)/SS(–) electrodes. The ElectraSyn vial was charged with compound **1** (0.4 mmol), TPPA (10 eq.), LiBr (7.5 eq.), DMU (3 eq.) and THF (14.4 mL), followed by constant-current electrolysis at 10 mA to a total charge of 25 F/mol. The reaction mixture was then subjected to a standard work-up to remove TPPA, LiBr, and DMU, after which TPPA and LiBr were reintroduced and electrolysis was resumed for an additional 10 F/mol in the absence of DMU. Error bars account for a 5% uncertainty. **Supporting Fig. S8**: Karl-Fischer coulometric titrator used for the determination of the amount of water in the system. **Supporting Fig. S9**: Kinetics of the electrochemical reduction of compound **1** using dry and non dry LiBr. Reactions were carried out in an undivided cell using an IKA ElectraSyn setup equipped with Mg(+)/Zn(–) electrodes. An ElectraSyn vial was charged with compound **1** (0.2 mmol), TPPA (10 eq.), LiBr (7.5 eq.), and dry THF (4 mL), followed by constant current electrolysis at 10 mA to a total charge of 25 F/mol. Prior to the reaction, LiBr was dried at high vacuum and 170°C during 24 h. Error bars account for a 5% uncertainty. **Supporting Fig. S10**: ^{31}P NMR spectra of the reaction carried out with tri(pyrrolidin-**1** yl)phosphine oxide (TPPA) and triphenylphosphine oxide (TPPO) at increasing charge inputs, showing that TPPA remains largely intact throughout electrolysis, whereas TPPO undergoes significant degradation under the same conditions. **Supporting Fig. S11**: a) Kinetics of the electrochemical reduction of compound **1**, using different starting concentrations. Reactions were carried out in an undivided cell using an IKA ElectraSyn setup equipped with Mg(+)/Zn(–) electrodes. The ElectraSyn vial was charged with compound **1** (0.1–0.3 mmol), TPPA (10 eq.), LiBr (7.5 eq.) and dry THF (4 mL), followed by constant-current electrolysis at 10 mA to a total charge of 5 F/mol. Error bars account for a 5% uncertainty. b) Starting speed of the reaction vs starting mmol of model compound **1**, according to the kinetics. **Supporting Fig. S12**: Kinetics of the electrochemical reduction of compound **1** at standard conditions (red line) compared to a reaction in which the current was stopped at 5 F/mol (black line). Reactions were carried out in an undivided cell

using an IKA ElectraSyn setup equipped with Mg(+)/Zn(−) electrodes. An ElectraSyn vial was charged with compound **1** (0.2 mmol), TPPA (10 eq.), LiBr (7.5 eq.), and dry THF (4 mL), followed by constant-current electrolysis at 10 mA to a total charge of 25 F/mol. Error bars account for a 5% uncertainty. **Supporting Fig. S13**: Isotopic labeling experiments. a) Electrochemical reduction of compound **1** performed in the presence of D2O (1–5 eq.), showing deuterium incorporation in the aliphatic fragment of the ring-opened product 2. b) Electrochemical reduction of compound **1** performed in THF-d8, in which no deuterium incorporation was detected. Reactions were carried out using Mg(+)/Zn(−) electrodes at 10 mA and 25 F/mol. In experiments employing 5 eq. of D2O, the amount of compound **1** was increased to 0.2 mmol in order to avoid a rapid increase in cell potential. **Supporting Fig. S14**: Mass chromatography spectrum of the deuterated product 2, with a +1 increase in mass respect to the non-deuterated product. **Supporting Fig. S15**: Kinetics of the electrochemical reduction of compound **1** using new and "dirty" electrodes. Reactions were carried out in an undivided cell using an IKA ElectraSyn setup equipped with Mg(+)/Zn(−) electrodes. The "dirty"ones were not cleaned from one reaction to another. An ElectraSyn vial was charged with compound **1** (0.2 mmol), TPPA (10 eq.), LiBr (7.5 eq.), and dry THF (4 mL), followed by constant current electrolysis at 10 mA to a total charge of 25 F/mol. Error bars account for a 5% uncertainty. **Supporting Fig. S16**: Kinetics of the electrochemical reduction of compound **1** changing the usual anode (Mg) to inactive ones (Zn) at 2.5 F/mol. Reactions were carried out in an undivided cell using an IKA ElectraSyn setup equipped with Mg(+)/Zn(−) electrodes, which were changed to Zn(+)/Zn(−) at 2.5 F/mol. An ElectraSyn vial was charged with compound **1** (0.2 mmol), TPPA (10 eq.), LiBr (7.5 eq.), and dry THF (4 mL), followed by constant current electrolysis at 10 mA to a total charge of 25 F/mol. Error bars account for a 5% uncertainty. **Supporting Fig. S17**: The Zn counter electrode (right) gets pasivated when adding a Mg^{2+} salt to the reaction (in this case $MgBr_2$) and a Mg electrode is used as a working electrode (Table S8, entry 6). **Supporting Fig. S18**: Cyclic voltammetry experiments where the voltammetric response is dominated by TPPA, which is present in excess and exhibits electroactivity within the explored potential window. **Supporting Fig. S19**: Reactivity of additional aryl ether substrates under the optimized conditions. Reactions were carried out in an undivided cell using an IKA ElectraSyn setup equipped with Mg(+)/Zn(−) electrodes. An ElectraSyn vial was charged with substrate (0.1 mmol), TPPA (10 eq.), LiBr (7.5 eq.), and dry THF (4 mL), followed by constant-current electrolysis at 10 mA to a total charge of 25 F/mol. All results are from GC and GC-MS. **Supporting Fig. S20**: ^{1}H, $^{13}C\{^{1}H\}$ and DEPT NMR spectrum of organosolv lignin, with peak assignments. **Supporting Fig. S21**: ^{1}H, $^{13}C\{^{1}H\}$ and DEPT NMR spectrum of organosolv lignin, with peak assignments. **Supporting Fig. S22**: ^{1}H, $^{13}C\{^{1}H\}$ and DEPT NMR spectra of lignin-derived fraction initially retained on silica, obtained after electrochemical treatment of organosolv lignin under the conditions described in Table S9 (entry 1), with some peak assignments. **Supporting Fig. S23**: ^{1}H, $^{13}C\{^{1}H\}$ and DEPT NMR spectra of lignin-derived fraction non-retained on silica, obtained after electrochemical treatment of organosolv lignin under the conditions described in Table S9 (entry 1), with some peak assignments. **Supporting Fig. S24**: IR FT-IR spectrum of reaction mixture (TPPA + lignin) before (blue line) and after (green and brown line) electrochemical reduction. **Supporting Fig. S25**: ^{1}H, $^{13}C\{^{1}H\}$ and DEPT NMR spectra of lignin-derived fraction initially retained on silica obtained after electrochemical treatment, with tentative signal assignments correlated with representative lignin-derived aromatic motifs. **Supporting Fig. S26**: ^{1}H, $^{13}C\{^{1}H\}$ and DEPT NMR spectra of lignin-derived fraction non-retained on silica obtained after electrochemical treatment, with tentative signal assignments correlated with representative lignin-derived aromatic motifs. Signals attributed to acetone and acetonitrile arise from residual solvents. **Supporting Fig. S27**: ^{1}H, $^{13}C\{^{1}H\}$ and DEPT NMR spectra of lignin-derived fractions obtained after electrochemical treatment of organosolv lignin under the conditions described in Table S9 (entry 2), with some peak assignments. **Supporting Fig. S28**: ^{1}H, $^{13}C\{^{1}H\}$ and DEPT NMR spectra of lignin-derived fractions obtained after electrochemical treatment of organosolv lignin under the conditions described in Table S9 (entry 3), with some peak assignments. **Supporting Fig. S29**: ^{1}H, $^{13}C\{^{1}H\}$ and DEPT NMR spectra of lignin-derived fractions obtained after electrochemical treatment of organosolv lignin under the conditions described in Table S9 (entry 4), with some peak assignments. **Supporting Table S1**: Water content of reaction components determined by Karl-Fischer titration. **Supporting Table S2**: Results of the electrochemical reduction of **1** using different electrode combinations. Reactions were carried out in an undivided cell using an IKA ElectraSyn setup. An ElectraSyn vial was charged with compound **1** (0.1 mmol), TPPA (10 eq.), LiBr (7.5 eq.), and THF (3.6 mL), followed by constant-current electrolysis at 10 mA to a total charge of 25 F/mol. **Supporting Table S3**: Results of the electrochemical reduction of **1** using different solvents. Reactions were carried out in an undivided cell using an IKA ElectraSyn setup equipped with Mg(+)/Zn(−) electrodes. An ElectraSyn vial was charged with compound **1** (0.1 mmol), TPPA (10 eq.), LiBr (7.5 eq.), and THF (3.6 mL), followed by constant-current electrolysis at 10 mA to a total charge of 25 F/mol. The use of acetonitrile led to formation of intractable reaction mixtures, while DMF resulted in rapid electrode passivation. Similarly, the cell potential in 1,4-dioxane rapidly increased to the voltage limit of the equipment, leading to premature termination of electrolysis. **Supporting Table S4**: Results of the electrochemical reduction of **1** using different electrolytes. Reactions were carried out in an undivided cell using an IKA ElectraSyn setup equipped with Mg(+)/Zn(−) electrodes. An ElectraSyn vial was charged with compound **1** (0.2 mmol), TPPA (10 eq.), electrolyte (7.5 eq.), and THF (4 mL), followed by constant current electrolysis at 10 mA to a total charge of 25 F/mol. The low yield observed with LiCl is likely influenced by the higher moisture content of the salt. Other electrolytes such as NaCl, NaBr, NaBF4 and NH4Br were found to be insufficiently soluble in THF. **Supporting Table S5**: Results of the electrochemical reduction of **1** with different amounts of TPPA. Reactions were carried out in an undivided cell using an IKA ElectraSyn setup equipped with Mg(+)/Zn(−) electrodes. An ElectraSyn vial was charged with compound 1 (0.2 mmol), TPPA (5-10 eq.), LiBr (7.5 eq.), and THF (4 mL), followed by constant-current electrolysis at 10 mA to a total charge of 25 F/mol. **Supporting Table S6**: Results of the electrochemical reduction of 1 with different currents. Reactions were carried out in an undivided cell using an IKA ElectraSyn setup equipped with Mg(+)/Zn(−) electrodes. An ElectraSyn vial was charged with compound 1 (0.1 mmol), TPPA (10 eq.), LiBr (7.5 eq.), H2O (1 eq.), and THF (4 mL), followed by constant-current electrolysis at 7.5-20 mA to a total charge of 25 F/mol. At 15 and 20 mA, the cell potential raised up to 30V (IKA's ElectraSyn upper limit), decreasing the effective current. **Supporting Table S7**: Results of the electrochemical reduction of 1 with different currents and concentration of 1. Reactions were carried out in an undivided cell using an IKA ElectraSyn setup equipped with Mg(+)/Zn(−) electrodes. An ElectraSyn vial was charged with compound 1 (0.1-0.2 mmol), TPPA (10 eq.), LiBr (7.5 eq.), and dry THF (4 mL), followed by constant-current electrolysis at 10-20 mA to a total charge of 10-25 F/mol. **Supporting Table S8**: Results of the electrochemical reduction of 1 with different additives. Reactions were carried out in an undivided cell using an IKA ElectraSyn setup equipped with the electrodes indicated in each case. An ElectraSyn vial was charged with compound **1** (0.2 mmol), TPPA (10 eq.), LiBr (7.5 eq.), and dry THF (4 mL), followed by constant-current electrolysis at 10 mA to a total charge of 25 F/mol. **Supporting Table S9**: Conditions of electrochemical experiments with organosolv lignin. Reactions were carried out in an undivided cell using an IKA ElectraSyn setup equipped with Mg(+)/cathode(−) electrodes. An ElectraSyn vial was charged with lignin organosolv (50 100 mg), TPPA (500 mg), LiBr (130 mg), and dry THF (4 mL), followed by constant current electrolysis during 14 h.